ACS MATERIALS LETTERS

www.acsmaterialsletters.org

Understanding the Double Doping of Organic Semiconductors Via State Energy Renormalization upon Charging

Ross Warren, Eunkyung Cho, Hong Li, Jean-Luc Bredas, and Norbert Koch*

Cite This: *ACS Materials Lett.* 2022, 4, 2051−2057

Read Online

ACCESS | Metrics & More | Article Recommendations

ABSTRACT: **The double ionization of molecular dopants enables the doping efficiency (free charges per dopant molecule) to rise above 100%. However, the current models of doped organic semiconductors based on Fermi−Dirac statistics fail to explain the double ionization of dopants and also the analogous situation of bipolaron formation on a host polymer. Here, we address this shortcoming by considering the renormalization of the state energies upon electron transfer between host and p-dopant. We vary the model parameters—the reorganization energy and evolutions of ionization energies and electron affinities upon charging—and plot the fractions of doubly ionized, singly ionized, and neutral species. The model shows good agreement with experimental measurements of doubly ionized p-dopants and bipolarons on a p-doped polymer. With these insights, we suggest that the state energy renormalization upon charging is the key parameter to be minimized for double ionization of dopants or maximized to avoid formation of bipolarons on the host.**

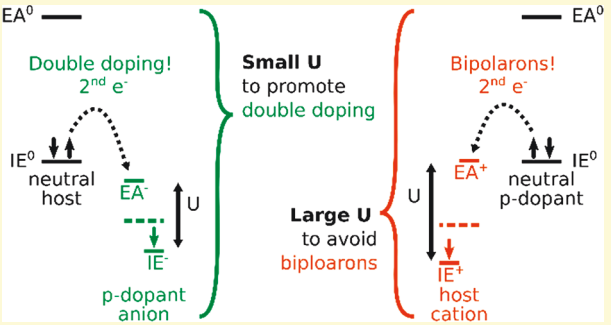

The addition of impurities (here dopant molecules) to a semiconductor can increase the conductivity of the material over many orders of magnitude. For redox p-doping of polymer semiconductors, this process involves two steps: electron transfer from the host polymer to a dopant molecule, followed by charge separation.[1−3] The mobile hole on the polymer then contributes to the increase in the material's conductivity. With this description, the most effective dopants generate one free carrier per dopant molecule (doping efficiency η = 100%). However, there are now reports of the double ionization of dopants,[4−6] where one dopant molecule generates two charge carriers. These results have two fundamental consequences. First, they allow for doping efficiencies to rise above 100%. This means high conductivity can be achieved with fewer dopant molecules, resulting in less disruption to the film's structure[7,8] and a smaller reduction in carrier mobility.[9−11] Second, they raise an issue with the current doping models,[1,3,12−16] where the host and dopant density of states (DOS) are only considered for the ground-state configuration, that is, *before* charge transfer. This prevents these models from describing the double ionization of dopants.

In fact, these models[1,3,12−16] estimate the density of charge carriers and ionized dopants in doped organic semiconductors based upon semiconductor physics developed for inorganic materials. The density of charge carriers on the host and the density of ionized dopants are calculated by multiplying the density of states by an occupation probability and integrating over energy. Such models have been found to reproduce the Fermi level shift as a function of dopant concentration[12,13] and doping efficiencies for various molecularly doped semiconductors.[14,15] These models can also account for the formation of ground-state integer charge-transfer complexes[3] and/or the hybridization of the frontier molecular orbitals of host and dopant.[1,16]

Here, we provide the necessary extension of these models to account for the experimental observation by Kiefer et al.[4] of doubly ionized dopant molecules. The extension considers state energy renormalization after the first electron transfer from host to dopant. This renormalization, based on Winkler et al.'s photoelectron spectroscopy study on p-doped C_{60},[17] includes (i) the reorganization of the molecules on account of

Received: July 10, 2022
Accepted: August 11, 2022
Published: September 14, 2022

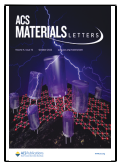

Downloaded via 80.187.86.138 on January 3, 2023 at 13:40:57 (UTC).
See https://pubs.acs.org/sharingguidelines for options on how to legitimately share published articles.

ACS Publications

© 2022 The Authors. Published by American Chemical Society

https://doi.org/10.1021/acsmaterialslett.2c00619
ACS Materials Lett. 2022, 4, 2051−2057

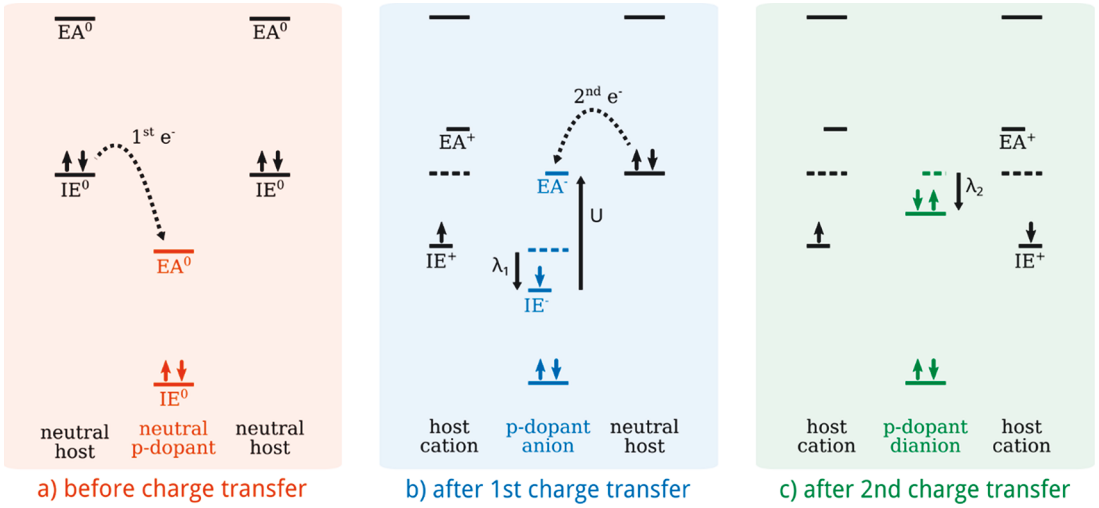

Figure 1. Change in state energies upon charging in a double doped organic semiconductor. (a) The configuration before charge transfer from the strong p-type dopant. (b) After the first charge transfer, the dopant anion's ionization energy IE^- shifts by the reorganization energy λ_1 relative to the neutral dopant's electron affinity EA^0. The dopant anion's electron affinity EA^- sits at energy U above IE^-. (c) After the second charge transfer, the dopant's now doubly occupied state again relaxes by λ_2 (Arrows denoting electrons are included to give an intuitive correspondence with molecular orbital models.).

becoming charged and (ii) the evolution of the ionization energies and electron affinities as a result of on-site Coulomb interactions upon charging. These changes in state energies are illustrated in Figure 1a–c, from the ground-state configuration in 1a, to single charge transfer in 1b and double ionization in 1c. The energies associated with the reorganization of the singly ionized and doubly ionized molecules are marked as λ_1 and λ_2, with the separation between the ionization energy and electron affinity of the singly ionized molecule corresponding to and labeled as Hubbard U.[18,19]

For an amorphous organic semiconductor film, we represent the relevant state energies using Normal distributions and calculate the occupation of each distribution by applying a charge neutrality condition—that the number density of charges on the polymer must equal the number density of charges on the dopant. We model how the fraction of singly ionized and doubly ionized dopants evolves as a function of dopant concentration and how these trends change with respect to the model parameters. The four model parameters that we assess are the energy offset between the host's and dopant's DOS, labeled E_{offset}, the standard deviation σ of the Normal distributions representing the DOSs, the reorganization energy λ of the molecules, and the energy difference U between the ionization energy and electron affinity of the singly ionized molecules. The λ and U values are estimated from long-range corrected density functional theory (DFT) calculations. Considering these parameter values, we find good agreement of the model to two sets of previously reported experimental data, one for a system showing double dopant ionization and another for bipolaron formation on a p-doped polymer host. Finally, we state that U is the key parameter to be minimized for double ionization of dopants or maximized to avoid the formation of bipolarons on the host.

We now turn to a description of the model and the methods for calculating λ and U. We first define the DOS as following Normal distributions, drawn for IE^0 and EA^0 energies in Figure 2a. With this description, the experimentally accessible parameters of IE^0_{exp} and EA^0_{exp} are defined by a linear extrapolation from the inflection point of the distribution toward $x = 0$. This places IE^0_{exp} and EA^0_{exp} at an energy 2σ away from the distributions centers.[2] For example, in the double doping case of Kiefer et al.,[4] the neutral p-dopant's EA^0_{exp} is 0.7 eV below the neutral host polymer's IE^0_{exp}. With an estimate of the standard deviation at σ = 0.15 eV, the center of the dopant's distribution of empty states, $g^{EA^0}_{dopant}$, sits 0.1 eV below the center of the host's distribution of occupied states, $g^{IE^0}_{host}$. This value of 0.1 eV will be used later in our model.

Next, we consider the effects of charge transfer between host and dopant on the DOS. In Figure 2b–g, we plot the DOSs, before and after state energy renormalization, and the final occupation of each distribution. We do this for strong p-type molecular doping, showing two cases for a low (0.5 mol %) and a high (25 mol %) dopant concentration. In Figure 2b,e, we draw the ground-state configuration (i.e., before charge transfer) with the neutral host's distribution of occupied states, labeled $g^{IE^0}_{host}$, and the neutral dopant's distribution of empty states, $g^{EA^0}_{dopant}$. In Figure 2c,f, we show how the dopant's DOS splits considering the state energy renormalization upon charge transfer. The DOS for the dopant anion's IE $g^{IE^-}_{dopant}$ shifts downward in energy by λ_1 relative to $g^{EA^0}_{dopant}$. The DOS for the dopant anion's EA $g^{EA^-}_{dopant}$ sits above $g^{IE^-}_{dopant}$ by the Hubbard U minus a second reorganization energy U-λ_2. In our modeling, we approximate $\lambda_1 \approx \lambda_2 = \lambda$. Finally, in Figure 2d,g, we calculate the number density in each distribution by taking the product of the DOS and the occupation probability $f(E)$ and integrating over energy. For example, the density of holes on the host p_{host} is calculated using the following integral

$$p_{host} = \int_{-\infty}^{\infty} g^{IE^0}_{host}(E)[1 - f(E, E_f)]\, dE$$

with the occupation probability given by the Fermi–Dirac distribution. The Fermi level E_f is set by the neutrality condition

$$p_{host} = n^{anion}_{dopant} + 2 \cdot n^{dianion}_{dopant}$$

https://doi.org/10.1021/acsmaterialslett.2c00619
ACS Materials Lett. 2022, 4, 2051–2057

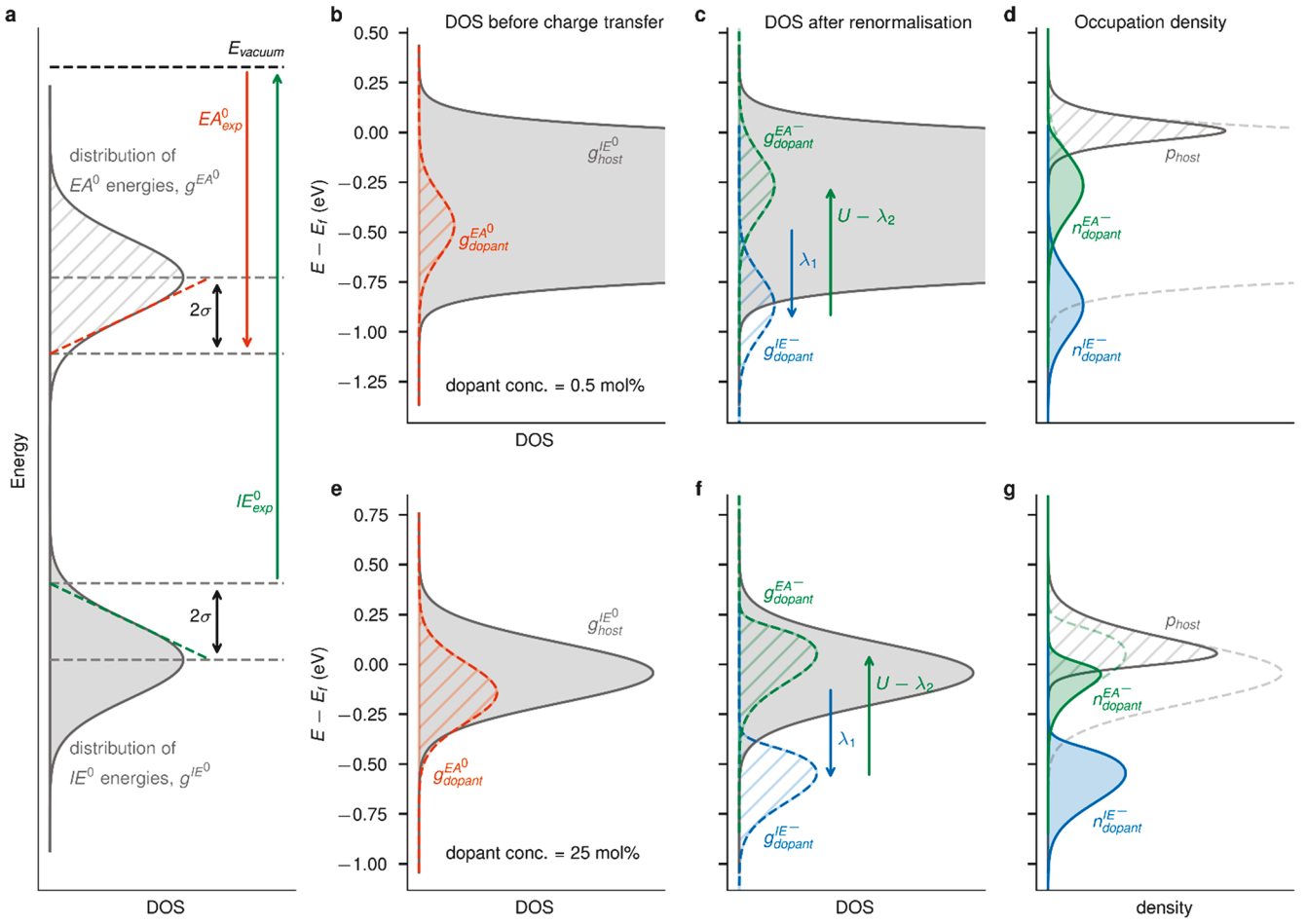

Figure 2. (a) The DOS for a neutral semiconductor's distributions of ionization energies g^{IE^0} and electron affinities g^{EA^0}, represented as Normal distributions. The experimentally accessible parameters of IE^0_{exp} and EA^0_{exp} are defined as shown, by a linear extrapolation from each distribution's inflection point. This definition places IE^0_{exp} and EA^0_{exp} at an energy 2σ away from the distribution's center. In the right-hand six panels: change in DOS upon charging in a (b–d) lightly and (e–g) heavily p-doped organic semiconductor. (b, e) The ground-state DOS for host and dopant. The filled color represents occupied states, and the hatch pattern represents unoccupied states. (c, f) The DOSs redrawn considering one charge transfer. $g^{IE^-}_{dopant}$ shifts down in energy by the reorganization energy λ_1, with the upper manifold, $g^{EA^-}_{dopant}$, separated by energy U-λ_2. (d, g) The occupation of the DOSs considering the shifts in energy upon charging. The electron densities are marked $n^{IE^-}_{dopant}$ and $n^{EA^-}_{dopant}$, and the host polymer's hole density is marked p_{host}. The parameters used to generate the six right-hand panels are set as T = 300 K, E_{offset} = −0.1eV, σ = 0.15eV, λ = 0.4eV, and U = 1.0 eV.

stating that the number density of holes on the host, p_{host}, is equal to the number densities of singly charged dopant anions n^{anion}_{dopant} plus twice the doubly charged dopant dianions $n^{dianion}_{dopant}$. Considering that $n^{anion}_{dopant} = n^{IE^-}_{dopant} - n^{EA^-}_{dopant}$ and $n^{dianion}_{dopant} = n^{EA^-}_{dopant}$, the neutrality condition, in terms of the quantities plotted in Figure 2, reads

$$p_{host} = n^{IE^-}_{dopant} + n^{EA^-}_{dopant}$$

With the model defined, we now discuss calculating λ and U. We evaluate λ and U for a representative host/dopant system at the DFT level. We consider a molecular complex consisting of the p-dopant 2,3,5,6-tetrafluoro-7,7,8,8tetracyanoquinodimethane (F4TCNQ) and a dimer of the bithiophene-thienothiophene polymer p(g42T-TT), see Figure 3. The complex is optimized at the unrestricted long-range corrected LC-ωhPBE/6-31G** level of theory with the GD3BJ dispersion correction. We account for the medium polarity (dielectric constant ε = 7) via the polarizable continuum model (PCM), in order to match the sample fabrication condition in a 1:1 $CH_3CN/CHCl_3$ mixture; we note that this approach was also applied in the earlier DFT calculations for double dopant systems.[4] We start with the molecular complex and each individual component in their neutral ground state, which we call the 0/0 complex. From the initial optimized geometries, we perform constrained-DFT calculations, at the same level of theory, with constraints of +1/−1 and +2/−2 charges on the dimer/F4TCNQ components in the complex, respectively. This allows us to evaluate the single and double dopant ionizations. Note that the total charge of the whole complex is set to zero. The U value is then estimated from

$$\begin{aligned} 2U_{complex} = {} & E[(\text{polymer}(+2) + \text{dopant}(-2)] \\ & + E[(\text{polymer}(0) + \text{dopant}(0)] \\ & - 2 \times E[(\text{polymer}(+1) + \text{dopant}(-1)] \end{aligned}$$

where 0, +1 (or +2), and −1 (or −2) represent the neutral, singly (or doubly) positively charged, and singly (or doubly) negatively charged states, respectively.

https://doi.org/10.1021/acsmaterialslett.2c00619
ACS Materials Lett. 2022, 4, 2051−2057

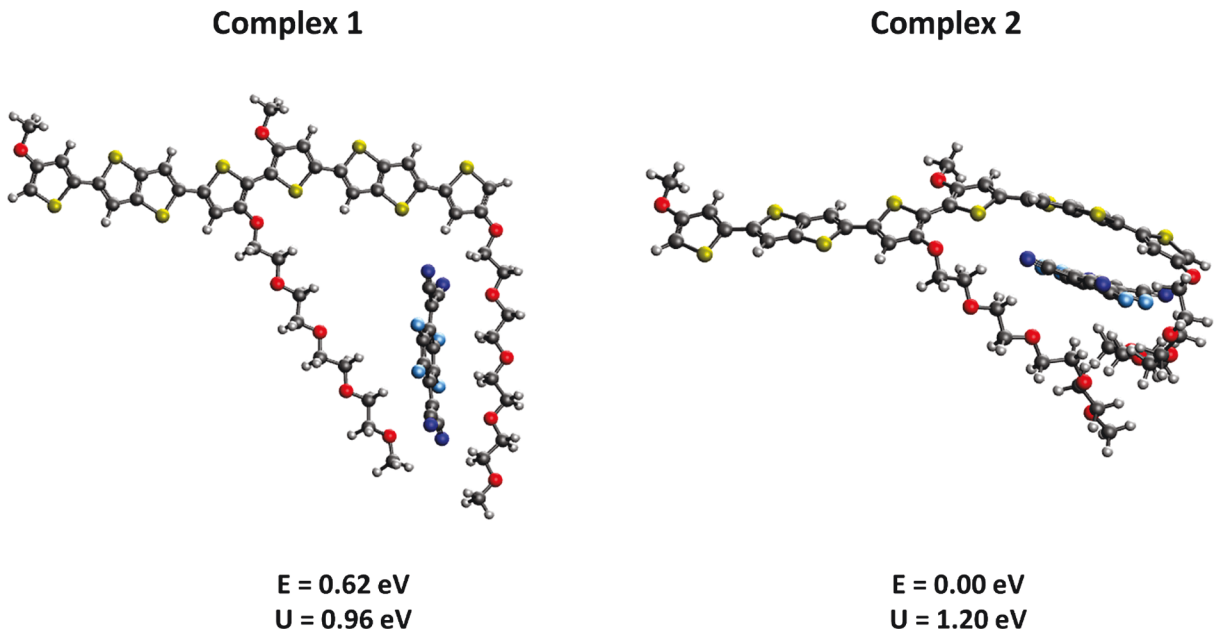

Figure 3. Molecular configurations of the p(g42T-TT) dimer/F4TCNQ system fully optimized in the overall neutral ground state at the unrestricted LC-ωhPBE/6-31G level of theory with the GD3BJ dispersion correction and $\varepsilon = 7$. The relative energy (E) and U values are given.**

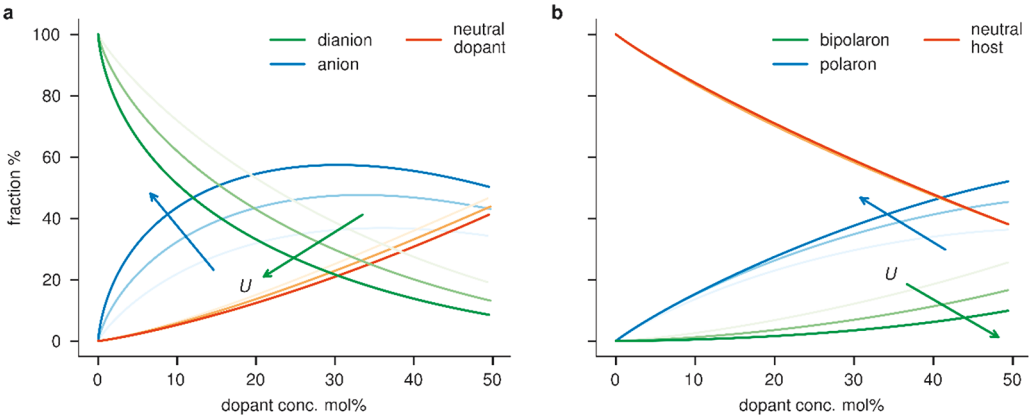

Figure 4. Fraction of doubly ionized, singly ionized, and neutral species as a function of molar dopant concentration (a) from the p-dopant side, (b) from the host side. The Hubbard energy is varied. U = 0.95, 1.00, and 1.05 eV with all other parameters constant: T = 300 K, E_{offset} = −0.1 eV, σ = 0.15 eV, and λ = 0.4 eV.

The reorganization energy (λ) of an isolated dopant F4TCNQ is evaluated at the same level of theory as for the complex. The total energies of the singly charged and neutral species of F4TCNQ, in each case on fully optimized geometries, are calculated to obtain the ionization energy (IE), electron affinity (EA) and, consequently, λ

$$\lambda_{dopant} = IE_{dopant}(-1) - EA_{dopant}(0)$$
$$= [E^0(-1) - E^{-1}(-1)] - [E^0(0) - E^{-1}(0)]$$

where $E^A(B)$ denotes the energy of the A charged species at the geometry optimized in the B state. All DFT calculations are carried out with the Gaussian 16 program,[20] with the exception of the constrained DFT calculations performed with the Q-Chem 5.3 package.[21]

Starting from several initial geometries of the dimer/F4TCNQ complex, two optimized configurations stand out, see Figure 3. The first, referred to as complex 1, has the dopant intercalated between the polymer side chains; this configuration is consistent with the experimental data and DFT calculations reported in ref 4. The complex 2 configuration has F4TCNQ lying flat on top of the polymer backbone, which maximizes the $\pi-\pi$ dispersion interactions. While, as a result, complex 2 is more stable than complex 1 by some 0.62 eV (ca. 14 kcal/mol), in practice, this configuration is less expected to appear, as it implies that the dopant has to separate interacting polymer backbones to intercalate in between them. Thus, our focus here is on complex 1, for which we calculate U to be 0.96 eV. The reorganization energy of the dopant, estimated from the difference between the vertical IE of the anion and the vertical EA of the neutral species, is λ = 0.39 eV.

In Figure 4a, we plot the fraction of dianions, anions, and neutral dopant molecules as a function of molar dopant concentration. We show the case for a strong p-type dopant, with the model parameters set identically as that for Figure 2. At very low dopant concentrations (below 1 mol %), all

https://doi.org/10.1021/acsmaterialslett.2c00619
ACS Materials Lett. 2022, 4, 2051−2057

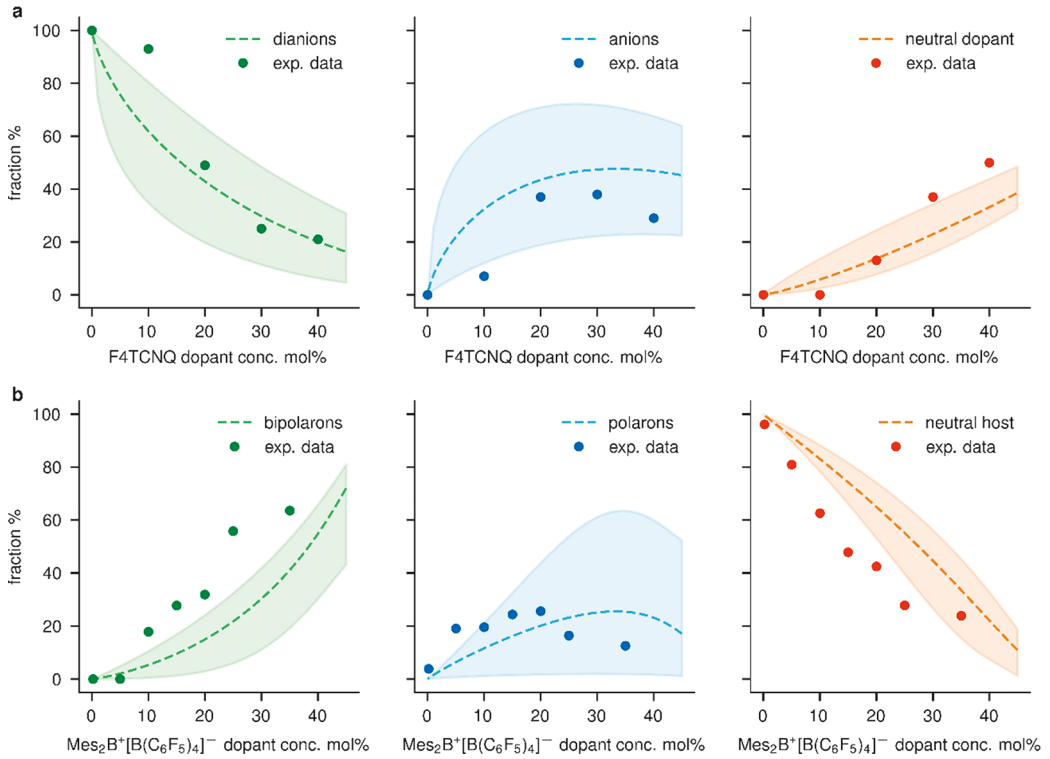

Figure 5. Model vs experimental data for two systems. (a) Dianions, anions, and neutral p-dopant molecules of F4TCNQ in polymer host p(g42T-TT). Experimental data from ref 4. (b) Bipolarons, polarons, and neutral host molecules of P3HT p-doped with $Mes_2B^+[B(C_6F_5)_4]^-$. Experimental data from ref 21. The shaded regions represent an estimate of uncertainty in the model.

dopants are doubly ionized with the Fermi level above both the dopant anion's $g^{EA^-}_{dopant}$ and $g^{IE^-}_{dopant}$ distributions. As the dopant concentration increases and the Fermi level shifts to within $g^{EA^-}_{dopant}$, the fraction of dianions decreases. At this point, $g^{IE^-}_{dopant}$ is still below the Fermi level and, so, remains filled. Therefore, the fraction of anions ($n^{IE^-}_{dopant} - n^{EA^-}_{dopant}$) begins to increase. At high dopant concentrations (above 10 mol %), the Fermi level drops to within $g^{IE^-}_{dopant}$. Decreasing occupation of the $g^{IE^-}_{dopant}$ distribution directly corresponds with a decreasing fraction of anions and an increasing fraction of neutral dopant molecules.

Next, we test how the splitting between the dopant's $g^{EA^-}_{dopant}$ and $g^{IE^-}_{dopant}$ distributions affect the fraction of dianions, anions, and neutral species as a function of dopant concentration. In Figure 4a, we vary U (0.95, 1.00, and 1.05 eV) with all other model parameters constant. The generation of dianions is favored with smaller U, as $g^{EA^-}_{dopant}$ shifts to lower energy and becomes more accessible.

We investigate the analogous situation of bipolaron formation on a polymer semiconductor. For these calculations, the neutrality condition is adjusted so that we also consider the densities in the host cation's occupied $p^{IE^+}_{host}$ and unoccupied $p^{EA^+}_{host}$ distributions as follows.

$$p^{IE^+}_{host} + p^{EA^+}_{host} = n^{IE^-}_{dopant} + n^{EA^-}_{dopant}$$

In Figure 4b, we plot the fraction of bipolarons, polarons, and neutral host molecules (neutral segments on the polymer) as a function of dopant concentration. For dopant concentrations below ~25 mol %, we see a linear increase in polaron formation. Above ~25 mol %, the fraction of bipolarons begins to increase. In terms of the Fermi level position, the formation of bipolarons occurs when the Fermi level shifts to sit within the host cation's distribution of singly occupied states, $g^{IE^+}_{host}$. Therefore, high dopant concentrations are required to generate bipolarons. Again, we vary U = 0.95, 1.00, 1.05 eV with all other model parameters constant. We find that bipolaron formation tends to be suppressed with increasing U.

We compare our model to experimental data from two previous studies. The first data set comes from UV−vis absorption measurements on thin films of p(g42T-TT)/F4TCNQ.[4] Kiefer et al. determined the fractions of dianions, anions, and neutral species of F4TCNQ by fitting absorption coefficients using the method of least-squares. We plot the experimental data as points in Figure 5a, with a panel for each species. We set the energy offset between the host and dopant manifolds by reference to cyclic voltammetry measurements[4] at E_{offset} = −0.1 eV. The standard deviation of the DOSs is estimated at σ = 0.15 eV. We vary the last two model parameters to best fit the experimental data, giving values of λ = 0.4 eV and U = 1.0 eV. These results are in remarkable agreement with the DFT-derived values of λ = 0.39 eV and U = 0.96 eV for complex 1, which supports that, in the double-doping system, the dopant intercalates in between the polymer side chains.

In Figure 5, we also display a shaded region to represent the sensitivity of the model to changes in the λ and U parameters. This region is determined by varying λ and U by ±0.05 eV and rerunning the calculations. Our best-fit parameters along with our uncertainty estimates are summarized in Table 1.

We repeat our fitting process using a second set of experimental data from ref 21. In the referenced report, bipolaron formation is observed in poly(3-hexylthiophene-2,5-

https://doi.org/10.1021/acsmaterialslett.2c00619
ACS Materials Lett. 2022, 4, 2051−2057

Table 1. Values of the Model Parameters Used to Fit the Experimental Data in Figure 5[a]

	E_{offset} (eV)	σ (eV)	λ (eV)	U (eV)
p(g42T-TT)/F4TCNQ	−0.10	0.15	0.40 ± 0.05	1.00 ± 0.05
P3HT/ $Mes_2B^+[B(C_6F_5)_4]^-$	−0.60	0.15	0.40 ± 0.05	0.90 ± 0.05

[a] E_{offset} and σ are fixed, while λ and U are varied freely. The uncertainty in λ and U corresponds to the lightly shaded regions in Figure 5.

diyl) (P3HT) heavily p-doped with an organic salt consisting of a diarylborinium ion (Mes_2B^+, Mes = mesityl) and a tetrakis(pentafluorophenyl)borate anion ($[B(C_6F_5)4]^-$) ($Mes_2B^+[B(C_6F_5)_4]^-$). Wegner et al.[22] determined the fractions of bipolarons, polarons, and neutral P3HT by an analysis of the sulfur core-level spectra as measured by X-ray photoemission spectroscopy. We plot these experimental data and our model fit in Figure 5b. As before, we observe good agreement between the trends in the experiment and the trends in the model. The best-fit values and uncertainty are summarized in Table 1.

Overall, the model with our values of λ and U produces trends that match the experimental data very well. Despite this, the model does neglect several physical details, which may be relevant for future work. For example, we do not consider entropic contributions that would promote charge transfer for cases where a dopant is surrounded by many host polymer segments. We speculate that ignoring entropy leads to an underestimation of charge transfer and of U. Also, we only consider energetic disorder and not spatial disorder. The molecular/polymer segment states represented by the Normal distributions in Figure 2 are disordered with respect to energy. However, in reality, these states may also be spatially separated. This puts an additional requirement on charge transfer between host and dopant—not only must the energetic offset be favorable for charge transfer but the states must also correspond to neighboring molecules. Again we speculate that neglect of spatial disorder leads to an overestimate of the charge transfer and of U, particularly for high dopant concentrations.

To conclude, we report that the double ionization of dopants can be understood by considering the change in state energies upon charging. We present a model that uses Normal distributions for the densities of states and Fermi−Dirac statistics to numerically solve for the Fermi level at each dopant concentration. Unlike previous models, which consider only the ground-state configuration, we allow the state energies to shift by λ and U upon charging. In this way, the model allows for the double ionization of the dopant and, analogously, bipolaron formation on the host. In combination with DFT estimates of λ and U, the model shows good agreement with experimental measurements of the fraction of dianions, anions, and neutral species in a p-doped sample. The model also shows good agreement with measurements of the fractions of bipolarons, polarons, and neutral species in a heavily p-doped P3HT film. Based on these findings, we suggest that the state energy renormalization upon charging is the key parameter to be either minimized for double ionization of dopants or maximized to avoid the formation of bipolarons on the host.

AUTHOR INFORMATION

Corresponding Author

Norbert Koch − *Institut für Physik & IRIS Adlershof, Humboldt-Universität zu Berlin, 12489 Berlin, Germany; Helmholtz-Zentrum Berlin für Materialien und Energie GmbH, 12489 Berlin, Germany;* orcid.org/0000-0002-6042-6447; Email: nkoch@physik.hu-berlin.de

Authors

Ross Warren − *Institut für Physik & IRIS Adlershof, Humboldt-Universität zu Berlin, 12489 Berlin, Germany;* orcid.org/0000-0002-9093-8347

Eunkyung Cho − *Department of Chemistry and Biochemistry, The University of Arizona, Tucson, Arizona 85721-0088, United States*

Hong Li − *Department of Chemistry and Biochemistry, The University of Arizona, Tucson, Arizona 85721-0088, United States;* orcid.org/0000-0002-4513-3056

Jean-Luc Bredas − *Department of Chemistry and Biochemistry, The University of Arizona, Tucson, Arizona 85721-0088, United States;* orcid.org/0000-0001-7278-4471

Complete contact information is available at: https://pubs.acs.org/10.1021/acsmaterialslett.2c00619

Notes

The authors declare no competing financial interest.

ACKNOWLEDGMENTS

The work in Berlin was supported by the Deutsche Forschungsgemeinschaft (Project No. 182087777-SFB951). The work at the University of Arizona was funded by the UA College of Science and the Office of Naval Research, Award No. N00014-20-1-2110. The authors acknowledge the use of High-Performance Computing (HPC) resources supported by Research Data Center (RDC) at the University of Arizona.

REFERENCES

(1) Salzmann, I.; Heimel, G.; Oehzelt, M.; Winkler, S.; Koch, N. Molecular Electrical Doping of Organic Semiconductors: Fundamental Mechanisms and Emerging Dopant Design Rules. *Acc. Chem. Res.* **2016**, *49*, 370−378.

(2) Scaccabarozzi, A. D.; Basu, A.; Aniés, F.; Liu, J.; Zapata-Arteaga, O.; Warren, R.; Firdaus, Y.; Nugraha, M. I.; Lin, Y.; Campoy-Quiles, M.; Koch, N.; Müller, C.; Tsetseris, L.; Heeney, M.; Anthopoulos, T. D. Doping Approaches for Organic Semiconductors. *Chem. Rev.* **2022**, *122*, 4420−4492.

(3) Tietze, M. L.; Benduhn, J.; Pahner, P.; Nell, B.; Schwarze, M.; Kleemann, H.; Krammer, M.; Zojer, K.; Vandewal, K.; Leo, K. Elementary Steps in Electrical Doping of Organic Semiconductors. *Nat. Commun.* **2018**, *9*, 1182.

(4) Kiefer, D.; Kroon, R.; Hofmann, A. I.; Sun, H.; Liu, X.; Giovannitti, A.; Stegerer, D.; Cano, A.; Hynynen, J.; Yu, L.; Zhang, Y.; Nai, D.; Harrelson, T. F.; Sommer, M.; Moulé, A. J.; Kemerink, M.; Marder, S. R.; McCulloch, I.; Fahlman, M.; Fabiano, S.; Müller, C. Double Doping of Conjugated Polymers with Monomer Molecular Dopants. *Nat. Mater.* **2019**, *18*, 149−155.

(5) Bathe, T.; Dong, C.-D.; Schumacher, S. Microscopic Study of Molecular Double Doping. *J. Phys. Chem. A* **2022**, *126*, 2075−2081.

(6) Järsvall, E.; Biskup, T.; Zhang, Y.; Kroon, R.; Barlow, S.; Marder, S. R.; Müller, C. Double Doping of a Low-Ionization-Energy Polythiophene with a Molybdenum Dithiolene Complex. *Chem. Mater.* **2022**, *34*, 5673−5679.

(7) Duong, D. T.; Wang, C.; Antono, E.; Toney, M. F.; Salleo, A. The Chemical and Structural Origin of Efficient P-Type Doping in P3HT. *Org. Electron.* **2013**, *14*, 1330−1336.
(8) Jacobs, I. E.; Aasen, E. W.; Oliveira, J. L.; Fonseca, T. N.; Roehling, J. D.; Li, J.; Zhang, G.; Augustine, M. P.; Mascal, M.; Moulé, A. J. Comparison of Solution-Mixed and Sequentially Processed P3HT:F4TCNQ Films: Effect of Doping-Induced Aggregation on Film Morphology. *J. Mater. Chem. C* **2016**, *4*, 3454−3466.
(9) Arkhipov, V. I.; Emelianova, E. V.; Heremans, P.; Bässler, H. Analytic Model of Carrier Mobility in Doped Disordered Organic Semiconductors. *Phys. Rev. B* **2005**, *72*, 235202.
(10) Pingel, P.; Schwarzl, R.; Neher, D. Effect of Molecular P-Doping on Hole Density and Mobility in Poly(3-Hexylthiophene). *Appl. Phys. Lett.* **2012**, *100*, 143303.
(11) Zuo, G.; Abdalla, H.; Kemerink, M. Impact of Doping on the Density of States and the Mobility in Organic Semiconductors. *Phys. Rev. B* **2016**, *93*, 235203.
(12) Tietze, M. L.; Burtone, L.; Riede, M.; Lüssem, B.; Leo, K. Fermi Level Shift and Doping Efficiency in p -Doped Small Molecule Organic Semiconductors: A Photoelectron Spectroscopy and Theoretical Study. *Phys. Rev. B* **2012**, *86*, 035320.
(13) Tietze, M. L.; Leo, K.; Lüssem, B. Quantification of Deep Hole-Trap Filling by Molecular p-Doping: Dependence on the Host Material Purity. *Org. Electron.* **2013**, *14*, 2348−2352.
(14) Tietze, M. L.; Pahner, P.; Schmidt, K.; Leo, K.; Lüssem, B. Doped Organic Semiconductors: Trap-Filling, Impurity Saturation, and Reserve Regimes. *Adv. Funct. Mater.* **2015**, *25*, 2701−2707.
(15) Warren, R.; Privitera, A.; Kaienburg, P.; Lauritzen, A. E.; Thimm, O.; Nelson, J.; Riede, M. K. Controlling Energy Levels and Fermi Level En Route to Fully Tailored Energetics in Organic Semiconductors. *Nat. Commun.* **2019**, *10*, 1−7.
(16) Salzmann, I.; Heimel, G.; Duhm, S.; Oehzelt, M.; Pingel, P.; George, B. M.; Schnegg, A.; Lips, K.; Blum, R.-P.; Vollmer, A.; Koch, N. Intermolecular Hybridization Governs Molecular Electrical Doping. *Phys. Rev. Lett.* **2012**, *108*, 035502.
(17) Winkler, S.; Amsalem, P.; Frisch, J.; Oehzelt, M.; Heimel, G.; Koch, N. Probing the Energy Levels in Hole-Doped Molecular Semiconductors. *Mater. Horiz.* **2015**, *2*, 427−433.
(18) Hubbard, J. Electron Correlations in Narrow Energy Bands. *Proc. R. Soc. London Ser. Math. Phys. Sci.* **1963**, *276*, 238−257.
(19) Schwedhelm, R.; Kipp, L.; Dallmeyer, A.; Skibowski, M. Experimental Band Gap and Core-Hole Electron Interaction in Epitaxial C 60 Films. *Phys. Rev. B* **1998**, *58*, 13176−13180.
(20) Frisch, M.; Trucks, G.; Schlegel, H.; Scuseria, G.; Robb, M.; Cheeseman, J.; Scalmani, G.; Barone, V.; Petersson, G.; Nakatsuji, H.; et al. *Gaussian 16;* Gaussian, Inc.: Wallingford, CT, 2016.
(21) Shao, Y.; Gan, Z.; Epifanovsky, E.; Gilbert, A. T.; Wormit, M.; Kussmann, J.; Lange, A. W.; Behn, A.; Deng, J.; Feng, X.; et al. Advances in Molecular Quantum Chemistry Contained in the Q-Chem 4 Program Package. *Mol. Phys.* **2015**, *113*, 184−215.
(22) Wegner, B.; Lungwitz, D.; Mansour, A. E.; Tait, C. E.; Tanaka, N.; Zhai, T.; Duhm, S.; Forster, M.; Behrends, J.; Shoji, Y.; Opitz, A.; Scherf, U.; List-Kratochvil, E. J. W.; Fukushima, T.; Koch, N. An Organic Borate Salt with Superior *p* -Doping Capability for Organic Semiconductors. *Adv. Sci.* **2020**, *7*, 2001322.

Recommended by ACS

Elucidating the Role of Disorder in Charge-Carrier Photoseparation in Organic Solar Cells
Mariusz Wojcik, Kazuhiko Seki, *et al.*
SEPTEMBER 15, 2022
THE JOURNAL OF PHYSICAL CHEMISTRY C
READ

Watching Polarons Move in the Energy and Frequency Domains Using Color Impedance Spectroscopy
Zhiting Chen and Erin L. Ratcliff
NOVEMBER 23, 2022
CHEMISTRY OF MATERIALS
READ

Ab Initio Molecular Dynamics Assessment on the Mixed Ionic–Electronic Transport for Crystalline Poly(3-Hexylthiophene) Using Full Explicit Lithium-Based Dopan...
Dominique Mombrú, Álvaro W. Mombrú, *et al.*
DECEMBER 29, 2021
MACROMOLECULES
READ

Structural and Dynamic Disorder, Not Ionic Trapping, Controls Charge Transport in Highly Doped Conducting Polymers
Ian E. Jacobs, Henning Sirringhaus, *et al.*
FEBRUARY 14, 2022
JOURNAL OF THE AMERICAN CHEMICAL SOCIETY
READ

Get More Suggestions >

https://doi.org/10.1021/acsmaterialslett.2c00619
ACS Materials Lett. 2022, 4, 2051−2057